Research Article | Vol. 8, No. 4 | 1 Apr 2017 | BIOMEDICAL OPTICS EXPRESS 2148
Biomedical Optics EXPRESS

Brain tumor delineation enhanced by moxifloxacin-based two-photon/CARS combined microscopy

VIET-HOAN LE,[1,5] SU WOONG YOO,[2,5] YEOREUM YOON,[3] TAEJUN WANG,[1] BUMJU KIM,[1] SEUNGHUN LEE,[3] KYUNG-HWA LEE,[4] KI HEAN KIM[1,3,6] AND EUIHEON CHUNG,[2,*]

[1]*Division of Integrative Biosciences and Biotechnology, Pohang University of Science and Technology, 77 Cheongam-Ro, Nam-gu, Pohang, Gyeongbuk 37673, South Korea*
[2]*Department of Biomedical Science and Engineering, Institute of Integrated Technology (IIT), Gwangju Institute of Science and Technology (GIST), 123 Cheomdangwagi-Ro, Buk-gu, Gwangju 61005, South Korea*
[3]*Department of Mechanical Engineering, Pohang University of Science and Technology, 77 Cheongam-Ro, Nam-gu, Pohang, Gyeongbuk 37673, South Korea*
[4]*Department of Pathology, Chonnam National University Hwasun Hospital and Medical School, 322 Seoyang-ro, Hwasun-eup, Hwasun-gun, Jeollanam-do 58128, South Korea*
[5]*Co-first authors with equal contribution*
[6]*Co-corresponding author: kiheankim@postech.ac.kr*
[*]*ogong50@gist.ac.kr*

Abstract: Delineating brain tumor margin is critical for maximizing tumor removal while sparing adjacent normal tissue for better clinical outcome. We describe the use of moxifloxacin-based two-photon (TP)/coherent anti-Stokes Raman scattering (CARS) combined microscopy for differentiating normal mouse brain tissue from metastatic brain tumor tissue based on histoarchitectural and biochemical differences. Moxifloxacin, an FDA-approved compound, was used to label cells in the brain, and moxifloxacin-based two-photon microscopy (TPM) revealed tumor lesions with significantly high cellular density and invading edges in a metastatic brain tumor model. Besides, label-free CARS microscopy showed diminishing of lipid signal due to the destruction of myelin at the tumor site compared to a normal brain tissue site resulting in a complementary contrast for tumor detection. This study demonstrates that moxifloxacin-based TP/CARS combined microscopy might be advantageous for tumor margin identification in the brain that has been a long-standing challenge in the operating room.

OCIS codes: (180.4315) Nonlinear microscopy; (170.3880) Medical and biological imaging; (170.4580) Optical diagnostics for medicine; (190.4390) Nonlinear optics, integrated optics.

References and links

1. A. F. Eichler, E. Chung, D. P. Kodack, J. S. Loeffler, D. Fukumura, and R. K. Jain, "The biology of brain metastases-translation to new therapies," Nat. Rev. Clin. Oncol. **8**(6), 344–356 (2011).
2. E. C. Kaal, M. J. Taphoorn, and C. J. Vecht, "Symptomatic management and imaging of brain metastases," J. Neurooncol. **75**(1), 15–20 (2005).
3. R. Soffietti, P. Cornu, J. Y. Delattre, R. Grant, F. Graus, W. Grisold, J. Heimans, J. Hildebrand, P. Hoskin, M. Kalljo, P. Krauseneck, C. Marosi, T. Siegal, and C. Vecht, "EFNS Guidelines on diagnosis and treatment of brain metastases: report of an EFNS Task Force," Eur. J. Neurol. **13**(7), 674–681 (2006).
4. N. Bergner, B. F. Romeike, R. Reichart, R. Kalff, C. Krafft, and J. Popp, "Tumor margin identification and prediction of the primary tumor from brain metastases using FTIR imaging and support vector machines," Analyst (Lond.) **138**(14), 3983–3990 (2013).
5. N. Sanai, M. Y. Polley, M. W. McDermott, A. T. Parsa, and M. S. Berger, "An extent of resection threshold for newly diagnosed glioblastomas," J. Neurosurg. **115**(1), 3–8 (2011).
6. W. C. Lin, S. A. Toms, M. Johnson, E. D. Jansen, and A. Mahadevan-Jansen, "In vivo brain tumor demarcation using optical spectroscopy," Photochem. Photobiol. **73**(4), 396–402 (2001).
7. F. K. Albert, M. Forsting, K. Sartor, H. P. Adams, S. Kunze, "Early postoperative magnetic resonance imaging

#282574 https://doi.org/10.1364/BOE.8.002148
Journal © 2017 Received 12 Dec 2016; revised 17 Feb 2017; accepted 17 Feb 2017; published 9 Mar 2017

Biomedical Optics EXPRESS

after resection of malignant glioma: objective evaluation of residual tumor and its influence on regrowth and prognosis," Neurosurgery **34**, 45–60 (1994).
8. P. A. Valdés, D. W. Roberts, F. K. Lu, and A. Golby, "Optical technologies for intraoperative neurosurgical guidance," Neurosurg. Focus **40**(3), E8 (2016).
9. I. J. Gerard, M. Kersten-Oertel, K. Petrecca, D. Sirhan, J. A. Hall, and D. L. Collins, "Brain shift in neuronavigation of brain tumors: A review," Med. Image Anal. **35**, 403–420 (2017).
10. Q. T. Nguyen and R. Y. Tsien, "Fluorescence-guided surgery with live molecular navigation--a new cutting edge," Nat. Rev. Cancer **13**(9), 653–662 (2013).
11. B. W. Pogue, S. Gibbs-Strauss, P. A. Valdés, K. Samkoe, D. W. Roberts, and K. D. Paulsen, "Review of Neurosurgical Fluorescence Imaging Methodologies," IEEE J. Sel. Top. Quantum Electron. **16**(3), 493–505 (2010).
12. C. Kut, K. L. Chaichana, J. Xi, S. M. Raza, X. Ye, E. R. McVeigh, F. J. Rodriguez, A. Quiñones-Hinojosa, and X. Li, "Detection of human brain cancer infiltration ex vivo and in vivo using quantitative optical coherence tomography," Sci. Transl. Med. **7**(292), 292ra100 (2015).
13. K. K. Kolste, S. C. Kanick, P. A. Valdés, M. Jermyn, B. C. Wilson, D. W. Roberts, K. D. Paulsen, and F. Leblond, "Macroscopic optical imaging technique for wide-field estimation of fluorescence depth in optically turbid media for application in brain tumor surgical guidance," J. Biomed. Opt. **20**(2), 026002 (2015).
14. F. Helmchen and W. Denk, "Deep tissue two-photon microscopy," Nat. Methods **2**(12), 932–940 (2005).
15. C. Ricard and F. C. Debarbieux, "Six-color intravital two-photon imaging of brain tumors and their dynamic microenvironment," Front. Cell. Neurosci. **8**, 57 (2014).
16. S. W. Perry, R. M. Burke, and E. B. Brown, "Two-photon and second harmonic microscopy in clinical and translational cancer research," Ann. Biomed. Eng. **40**(2), 277–291 (2012).
17. W. R. Zipfel, R. M. Williams, and W. W. Webb, "Nonlinear magic: multiphoton microscopy in the biosciences," Nat. Biotechnol. **21**(11), 1369–1377 (2003).
18. G. Thomas, J. van Voskuilen, H. C. Gerritsen, and H. J. Sterenborg, "Advances and challenges in label-free nonlinear optical imaging using two-photon excitation fluorescence and second harmonic generation for cancer research," J. Photochem. Photobiol. B **141**, 128–138 (2014).
19. J. M. Dela Cruz, J. D. McMullen, R. M. Williams, and W. R. Zipfel, "Feasibility of using multiphoton excited tissue autofluorescence for in vivo human histopathology," Biomed. Opt. Express **1**(5), 1320–1330 (2010).
20. C. W. Freudiger, R. Pfannl, D. A. Orringer, B. G. Saar, M. Ji, Q. Zeng, L. Ottoboni, Y. Wei, C. Waeber, J. R. Sims, P. L. De Jager, O. Sagher, M. A. Philbert, X. Xu, S. Kesari, X. S. Xie, and G. S. Young, "Multicolored stain-free histopathology with coherent Raman imaging," Lab. Invest. **92**(10), 1492–1502 (2012).
21. T. T. Le, C. W. Rehrer, T. B. Huff, M. B. Nichols, I. G. Camarillo, and J. X. Cheng, "Nonlinear optical imaging to evaluate the impact of obesity on mammary gland and tumor stroma," Mol. Imaging **6**(3), 205–211 (2007).
22. H. Wang, Y. Fu, P. Zickmund, R. Shi, and J. X. Cheng, "Coherent anti-stokes Raman scattering imaging of axonal myelin in live spinal tissues," Biophys. J. **89**(1), 581–591 (2005).
23. C. L. Evans, X. Xu, S. Kesari, X. S. Xie, S. T. Wong, and G. S. Young, "Chemically-selective imaging of brain structures with CARS microscopy," Opt. Express **15**(19), 12076–12087 (2007).
24. M. Ji, S. Lewis, S. Camelo-Piragua, S. H. Ramkissoon, M. Snuderl, S. Venneti, A. Fisher-Hubbard, M. Garrard, D. Fu, A. C. Wang, J. A. Heth, C. O. Maher, N. Sanai, T. D. Johnson, C. W. Freudiger, O. Sagher, X. S. Xie, and D. A. Orringer, "Detection of human brain tumor infiltration with quantitative stimulated Raman scattering microscopy," Sci. Transl. Med. **7**(309), 309ra163 (2015).
25. M. Ji, D. A. Orringer, C. W. Freudiger, S. Ramkissoon, X. Liu, D. Lau, A. J. Golby, I. Norton, M. Hayashi, N. Y. R. Agar, G. S. Young, C. Spino, S. Santagata, S. Camelo-Piragua, K. L. Ligon, O. Sagher, and X. S. Xie, "Rapid, label-free detection of brain tumors with stimulated Raman scattering microscopy," Sci. Transl. Med. **5**(201), 201ra119 (2013).
26. T. Wang, W. H. Jang, S. Lee, C. J. Yoon, J. H. Lee, B. Kim, S. Hwang, C.-P. Hong, Y. Yoon, G. Lee, V.-H. Le, S. Bok, G.-O. Ahn, J. Lee, Y. S. Gho, E. Chung, S. Kim, M. H. Jang, S.-J. Myung, M. J. Kim, P. T. C. So, and K. H. Kim, "Moxifloxacin: Clinically compatible contrast agent for multiphoton imaging," Sci. Rep. **6**, 27142 (2016).
27. D. P. Kodack, E. Chung, H. Yamashita, J. Incio, A. M. Duyverman, Y. Song, C. T. Farrar, Y. Huang, E. Ager, W. Kamoun, S. Goel, M. Snuderl, A. Lussiez, L. Hiddingh, S. Mahmood, B. A. Tannous, A. F. Eichler, D. Fukumura, J. A. Engelman, and R. K. Jain, "Combined targeting of HER2 and VEGFR2 for effective treatment of HER2-amplified breast cancer brain metastases," Proc. Natl. Acad. Sci. U.S.A. **109**(45), E3119–E3127 (2012).
28. K. S. Madden, M. L. Zettel, A. K. Majewska, and E. B. Brown, "Brain tumor imaging: live imaging of glioma by two-photon microscopy," Cold Spring Harb. Protoc. **2013**(3), pdb.prot073668 (2013).
29. Y. Fu, T. B. Huff, H. W. Wang, H. Wang, and J. X. Cheng, "Ex vivo and in vivo imaging of myelin fibers in mouse brain by coherent anti-Stokes Raman scattering microscopy," Opt. Express **16**(24), 19396–19409 (2008).
30. S. Lee, J. H. Lee, J. H. Park, Y. Yoon, W. K. Chung, H. Tchah, M. J. Kim, and K. H. Kim, "In vivo 3D measurement of moxifloxacin and gatifloxacin distributions in the mouse cornea using multiphoton microscopy," Sci. Rep. **6**, 25339 (2016).
31. M. Olivo and B. C. Wilson, "Mapping ALA-induced PPIX fluorescence in normal brain and brain tumour using confocal fluorescence microscopy," Int. J. Oncol. **25**(1), 37–45 (2004).
32. W. Stummer, "Fluorescein in brain metastasis and glioma surgery," Acta Neurochir. (Wien) **157**(12), 2199–2200

Biomedical Optics EXPRESS

(2015).
33. F. Van Bambeke and P. M. Tulkens, "Safety profile of the respiratory fluoroquinolone moxifloxacin: comparison with other fluoroquinolones and other antibacterial classes," Drug Saf. **32**(5), 359–378 (2009).
34. R. C. Owens, Jr. and P. G. Ambrose, "Antimicrobial safety: focus on fluoroquinolones," Clin. Infect. Dis. **41**(Suppl 2), S144–S157 (2005).
35. P. Ball, R. Stahlmann, R. Kubin, S. Choudhri, and R. Owens, "Safety profile of oral and intravenous moxifloxacin: cumulative data from clinical trials and postmarketing studies," Clin. Ther. **26**(7), 940–950 (2004).
36. L. Qiao, X. Cui, and Y. Li, "Status epilepticus attributed to moxifloxacin in an adolescent patient with spina bifida occulta," Eur. J. Clin. Pharmacol. **67**(1), 103–104 (2011).
37. J. Shi and H. Xu, "Moxifloxacin Induced Seizures -A Case Report," Iran. J. Public Health **43**(9), 1291–1294 (2014).

1. Introduction

Brain metastasis is an important cause of morbidity and mortality for cancer patients with solid tumors [1]. It occurs in 15-25% of patients with cancer and exceeds the number of primary brain tumors at least four fold [2,3]. Scattered cancer cells from other parts of the body may pass through the blood-brain barrier, enter the brain parenchyma, and form metastatic colonies [4]. The percentage of tumor that has been removed during surgery is an important prognostic factor [5]. Currently, brain tumor margins are determined by neurosurgeons based on visual inspection and information provided by surgical navigation systems using computerized tomography (CT), magnetic resonance (MR) images, and/or intraoperative ultrasounds (IOUS) [6]. Still, it has been challenging to differentiate tumor margin due to limited resolution of these techniques [7]. Although on-site histopathology provides an accurate diagnosis, it is time-consuming and expensive. Thus, there exists a clinical demand of better approaches for precise tumor margin delineation with advanced optical imaging modality.

Optical techniques are useful for brain tumor surgery by providing real-time intraoperative information and various contrasts [8]. Brain tumor location is usually shifted during surgery, because brain tissue sinks and deforms due to its high compliance [9]. Fluorescein and 5-ALA, which are fluorescent dyes, are currently used to guide the location of tumors during surgery [10, 11]. Other optical imaging techniques have been developed to be used for delineating tumor from the normal at the resection field based on various optical properties. Optical coherence tomography (OCT) is a 3D imaging modality based on light scattering, and has detected tumors based on their high scattering properties compared to the normal [12]. Diffuse reflectance imaging measures the scattering and absorption properties of tissues, and was used to detect tumor margins [13]. Combination of autofluorescence and diffuse reflectance imaging was used to enhance the detection efficiency by using multiple contrasts [6]. However, these optical methods have limited image resolutions or biochemical contrast.

Microscopy techniques have better accuracy by providing high-resolution images down to the cellular level. Although on-site histopathology provides an accurate diagnosis, it is time-consuming. Thus there exists a clinical demand of better approaches for precise tumor margin delineation with advanced optical imaging modality. Over the past decades, new advanced optical microscopy techniques using nonlinear light-matter interactions to generate signal contrast have been developed [14]. Two-photon microscopy (TPM) has been widely used for translational and clinical cancer research [15, 16]. TPM uses either exogenous markers or endogenous contrasts including autofluorescence (AF) [17]. AF has typically been used for clinical application as many fluorescent markers have been limited due to biocompatibility issue. However TPM imaging with AF usually requires higher excitation laser power and longer pixel dwell time due to weak signal [18, 19]. Hence, a simple and clinically applicable contrast agent that is brighter than AF would be beneficial in cancer imaging.

Coherent anti-Stokes Raman scattering (CARS) microscopy is another nonlinear imaging modality that can be used for chemically-selective imaging of brain tumors. CARS

Biomedical Optics EXPRESS

microscopy is based on intrinsic vibrational properties of the molecules and thus does not require staining or labeling [20]. In CARS microscopy, a pump field $E_p(\omega_p)$ and a Stokes field $E_s(\omega_s)$ interact with the molecules in samples through a four-wave mixing process. When the beat frequency (ω_p - ω_s) matches the vibrational frequency of a molecule, a strong anti-Stokes field E_{as} at frequency $2\omega_p$ - ω_s is generated. For brain imaging, the beat frequency is usually tuned to 2845 cm^{-1} to detect lipids in the myelin membrane where CARS signal is from symmetric stretching vibration of C-H bonds in CH_2 functional groups of lipids. CARS microscopy has been used to identify lipid changes within tumor microenvironment during high-fat diet [21], to image myelin sheaths in nervous systems [22], and to differentiate between normal and malignant brain tissue [23]. With the capability of providing molecular information at sub-cellular resolution, CARS microscopy can augment information of traditional histopathology techniques. Stimulated Raman scattering (SRS) microscopy, which is another coherent Raman scattering microscopy technique without non-resonant background, was developed. Spectroscopic SRS microscopy, which can image multiple Raman vibrational bands, was applied to brain tumor and delineated tumor from normal tissue based on both relatively high protein and low lipid signals [24, 25].

We recently reported that moxifloxacin hydrochloride, an FDA-approved antibiotic compound, can be used as a biocompatible contrast agent for TPM imaging of cells in tissues by providing an excellent fluorescence contrast surpassing the weak AF [26]. Here we provide an evidence that the use of moxifloxacin in TPM can help reveal tumor margin in a metastatic brain tumor setting. Furthermore, this delineation of tumor can be further complemented by a combined modality with CARS microscopy which provides a myelin-specific contrast in central nervous tissue. For this study, we developed a simple brain metastasis model with a calvarial door approach.

2. Materials and methods

2.1 Two-photon (TP)/CARS microscopy setup

Simultaneous moxifloxacin applied TPM and CARS microscopy was performed using a custom-built system described in Fig. 1. The excitation beam for TPM was a femtosecond Ti:Sapphire laser (Chameleon Ultra II, Coherent, CA, USA), and this laser was used for the pump beam for CARS imaging. The Stokes beam for CARS imaging was generated from an optical parametric oscillator (OPO) (Chameleon, APE, Berlin, Germany), pumped by the Ti:Sapphire laser. To enhance the CARS signal, a 3 nm bandpass filter (F1, Semrock, NY, USA) was added to the Stokes beam line. The pump beam was kept unchanged to maximize the two-photon (TP) excitation of moxifloxacin. Wavelengths of the two beams were tuned to 808 nm for the pump beam and 1049 nm for the Stokes beam to make a frequency difference of 2843 cm^{-1}, corresponding to CH_2 symmetric stretching mode. The two laser beams were set at parallel polarization and temporally overlapped using delay lines DL1 and DL2, and then combined using a long-pass dichroic mirror DM1 (T860LPXR, Chroma, VT, USA). The collinearly combined beams were relayed to an objective lens after passing through a galvanometric scanning unit. The objective lens was 40 × , 1.1 NA (LD C-Apochromat 40 × /1.1, ZEISS) for high magnification imaging and 20 × , 1.1 NA (XLUMPLFLN, NA 1, Olympus) for wide field of view (FOV) imaging. The combined laser power of pump beam and Stokes beam was 17.5 mW on the sample surface. Epi moxifloxacin and CARS signals were collected by the same objective lens and separated by a long-pass dichroic mirror DM3 (T630LPXR, Chroma, VT, USA). Then the signals were detected by two photomultiplier tubes (PMT1 and PMT2, R298P, Hamamatsu, Tokyo, Japan) after filtered with a 550/100 nm bandpass detection filter (F3) for moxifloxacin signal and 680 short-pass filter (F2) for CARS signal. The pixel dwell time was set at 25 μs and the images were acquired at 150 μm × 150 μm FOV in the x-y plane with 512 pixels × 512 pixels or 256 pixels × 256 pixels. Total time to acquire one x-y frame was 6.5 seconds for 512 pixels × 512 pixels image and 3.25 seconds

Biomedical Optics EXPRESS

for 256 pixels × 256 pixels image. For each imaging session, the live, fast scanning imaging was performed at the speed of 3.25 seconds per frame to scan the whole sample surface to locate the region of interest. After acquisition, the raw data was processed to get color encoded images by a custom-built Matlab program (Matlab R2015a, Mathworks, MA, USA).

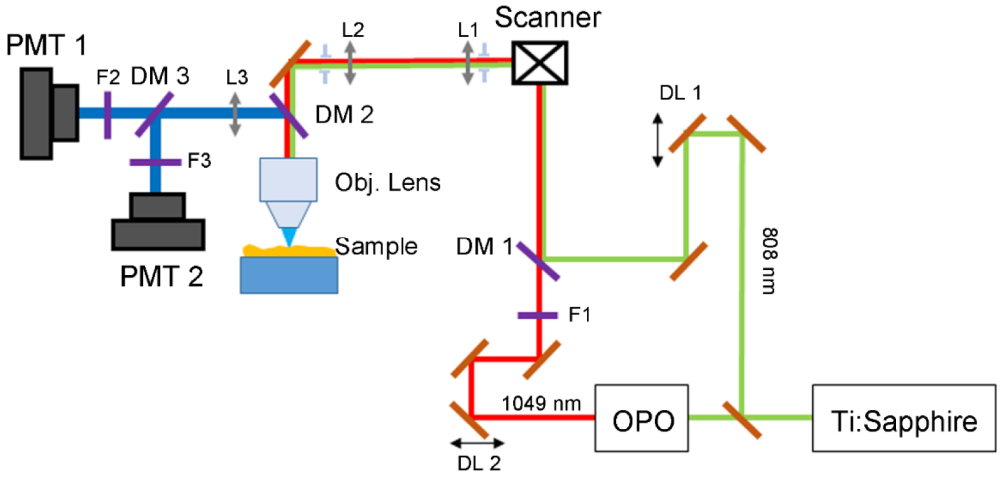

Fig. 1. Schematic of the TP/CARS combined microscopic system. The system uses Ti:Sapphire and OPO to produce 808 nm and 1049 nm beams as the pump and Stokes beams. Moxifloxacin signal and CARS signal are collected backward using objective lens and two photomultiplier tubes. SBS: beam splitter; OPO: optical parametric oscillator; DL1, DL2: delay lines; DM1, DM2, DM3: dichroic mirror; F1: 3nm narrow bandpass filter; F2, F3: detection bandpass filter; L1, L2, L3: lens; PMT: photomultiplier tube.

Large FOV moxifloxacin based TP imaging of brain tumor tissues, containing DsRed cancer cells, was conducted by using a commercial TPM (TCS SP5 II MP, Leica, Wetzlar, Germany) equipped with a Ti:Sapphire laser (Chameleon Vision II, Coherent, CA, USA). Excitation wavelength was selected at 830 nm to simultaneously excite both moxifloxacin and DsRed with deep tissue penetration. A 20x objective lens (HCX APO L20x 1.0NA, water immersion, Leica, Wetzlar, Germany) was used with z stepwise increment of 2 μm for 3D imaging. By using a set of dichroic mirrors and band-pass filters, emission light was spectrally resolved to 2 channels, 495 nm - 560 nm for moxifloxacin and 560 nm - 620 nm for DsRed, and detected by photomultiplier tubes (R10467U-40, Hamamatsu Tokyo, Japan). Each image contains 1024 pixels × 1024 pixels with FOV of 775 μm × 775 μm. The imaging speed was 0.1 frame per second including 2 line averaging and 2 frame accumulation. In order to enable large-area imaging, nine images were taken using an x-y translational stage and carefully stitched together manually.

2.2 Normal mouse brain tissue preparation

This study was approved by the Institutional Animal Care and Use Committee board of the Pohang University of Science and Technology (POSTECH-2015-0030-C1). Mouse models were bred at the animal facility of POSTECH Biotech Center under specific pathogen-free (SPF) condition. Six-week-old, three C57BL/6 mice were used. The brain tissue was extracted from the skull right after sacrifice. The brain tissue was sectioned in the coronal plane in 1 mm thickness with a surgical razor blade after 5 minutes of hardening in a freezer at − 20 °C. Moxifloxacin ophthalmic solution (0.5%, Vigamox, Alcon, TX, USA) was dropped over the sectioned brain tissue followed by incubation for 20 minutes at room temperature. After the incubation period, the remnant moxifloxacin was washed out with PBS 1 × and then the tissue was imaged with TP/CARS microscope system. After locating the hippocampus and subcortical white matter areas by performing the live and fast scanning

Biomedical Optics EXPRESS

imaging, the 2 by 2 mosaic image covering an area of 300 μm × 300 μm was acquired. Hematoxylin and Eosin (H & E) staining was used to characterize cellular structure of the examined tissue sample.

2.3 Cell preparation for brain tumor models

Highly metastatic colon cancer cells, SL4-DsRed, were kindly provided by the Edwin L. Steel Laboratory (Massachusetts General Hospital and Harvard Medical School, MA, USA). SL4-DsRed cells were cultured in Dulbecco's modified Eagle's Medium/Ham's F-12 (DMEM/F12) 1:1 medium supplemented with L-glutamine and 2.438 g/L $NaHCO_3$, 10% fetal bovine serum (FBS), 1% penicillin/streptomycin solution. All the media and reagents were purchased from Gibco (Invitrogen Corporation, NY, USA).

2.4 Development of metastatic brain tumor models: a calvarial door approach

Five-week-old, ten C57BL/6 mice were acclimatized for one week before use as described in Fig. 2. As spontaneous or hematogenous brain metastasis models are difficult to control for their occurrence and locations, an implanted brain metastasis is a feasible model for this experimental study [27]. Initial steps of the surgical procedure are similar to those of cranial window procedure [28]. The hair of the skull was shaved and cleared with hair removal cream under anesthesia with a Zoletil/xylazine mixture in saline solution (60/10 mg/kg body weight) (Figs. 2(b)-2(e)). After making a longitudinal incision of the scalp between the occiput and the forehead, underlying periosteum was scraped off to the temporal crests (Fig. 2(e)). A rectangle with 3 mm × 3 mm size was marked over the left parietal region of the skull (Fig. 2(f)). Using a sterile dental drill, three deep grooves and one shallow groove along each side of drawn rectangle were made (Fig. 2(g)). With repetitive gentle drilling, a door-like bony window (a calvarial door), was created. After opening the calvarial door, SL4-DsRed cancer cells (1×10^5 cells, suspended in 10 μL of phosphate buffered saline (PBS 1 ×)) were injected into the center of the craniotomy site at the depth of approximately 1.5 – 2.5 mm from the cortical surface by using a low-volume Hamilton syringe (Figs. 2(h) and 2(i)). After gentle injection, the craniotomy site was washed with PBS to prevent extra cerebral tumor growth and the calvarial door was closed. Finally, the scalp was sutured with surgical suture filaments (Vicryl 6-0, Ethicon Inc., Guaynabo, Puerto Rico).

2.5 Ex vivo imaging of moxifloxacin-based TP/CARS microscopy in a metastatic brain tumor model

Six mice bearing metastatic brain tumor were sacrified 7 days after cancer cell injection. The brain tissue was extracted right after sacrifice. The brain tissue slice was prepared and moxifloxacin was applied as described in section 2.2. Each sample was first imaged with the commercial TPM to get large FOV images with moxifloxacin and DsRed fluorescence, and then imaged with TP/CARS microscope system to obtain simultaneous moxifloxacin/CARS images. For TP/CARS imaging, after locating the tumor margin region by performing the live and fast scanning imaging, the 2 by 3 mosaic image covering an area of 300 μm × 450 μm was acquired. H & E staining was applied to the examined tissue sample.

Biomedical Optics EXPRESS

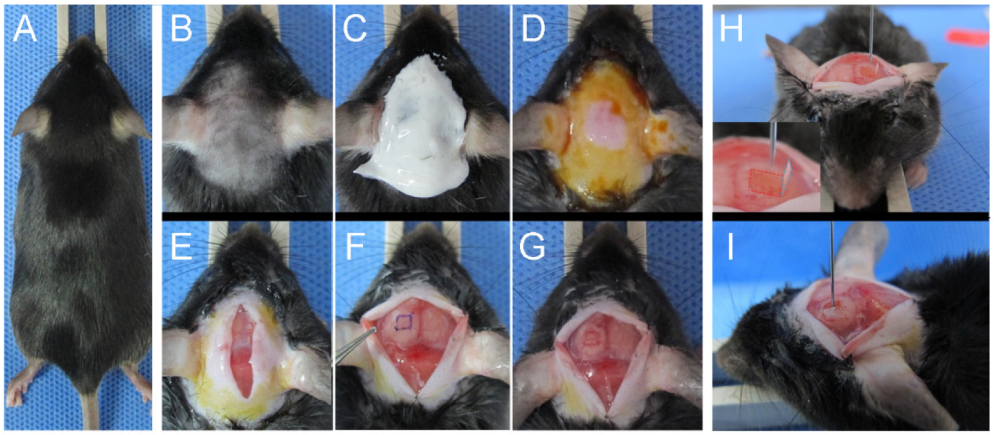

Fig. 2. Development of metastatic brain tumor model with a calvarial door (A) Image of an anesthetized C57BL/6 mouse. (B-D) Hair removal and preparation of the surgical site. (E) Incision of the scalp tissue. (F) Marking a rectangle on the left parietal lobe. (G) Making grooves along the edges of the rectangle with a dental drill. (H) Opened state of the calvarial door. Inset: magnified image of calvarial door. (I) Intracerebral injection of cancer cells with 28-gauge needle Hamilton syringe.

3. Results

3.1 Imaging mouse normal brain with moxifloxacin-based TP/CARS microscopy

Figure 3 shows mouse brain tissue imaging with TP/CARS microscopy after applying moxifloxacin. Moxifloxacin-based TP images showed multiple, neuronal cells in the hippocampus and subcortical white matter as well as myelinated fiber tracts (Figs. 3(a) and 3(d)). In contrast, those cells were not visible in CARS images. On the other hand, CARS images showed myelinated neural fibers more clearly than TP images (Figs. 3(b) and 3(e)). Correlated Fig. 3(h) and 3(e) image showed similar cellular distribution with TP images and fiber tract distribution with CARS images (Figs. 3(c) and 3(f)). This demonstrates the complementary nature of TPM and CARS microscopy in brain tissue imaging providing rich structural and chemical information.

3.2 Imaging mouse metastatic brain tumor with moxifloxacin-based TP/CARS microscopy

We obtained TP/CARS images from tumoral infiltrated lesion with histologic analysis. TP image showed high cellular density lesion on the left imaging fields, compared with right side (Fig. 4(a)). CARS image showed loss of myelination on the left side. However, it was difficult to define the tumor margin (Fig. 4(b)). Figures 4(h) and 4(e) stained tissue image showed tumoral infiltration on the left side of imaging fields (Fig. 4(c)). Multiple cancer cells (red arrow heads in Fig. 4(c)) and peritumoral immune cell infiltrations (blue arrows in Fig. 4(c)) were detected. With confirmation of correlated histologic staining, we can demonstrate the usefulness of moxifloxacin-based TPM and complimentary role of CARS microscopy.

Biomedical Optics EXPRESS

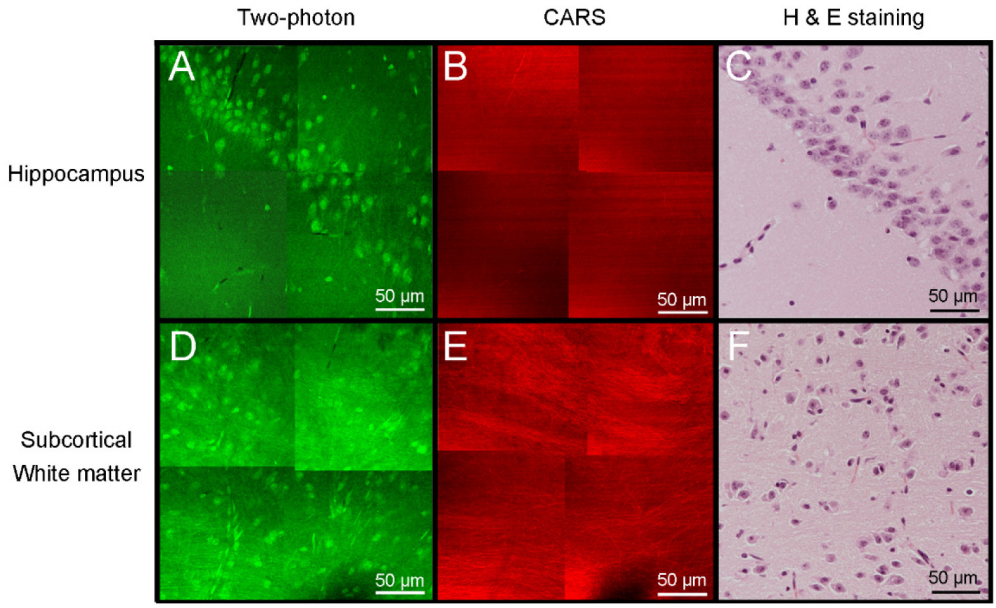

Fig. 3. TP/CARS microscopic images of hippocampus and cerebral cortex in normal mouse after application of moxifloxacin. Hippocampal images by (A) TPM and (B) CARS microscopy. (C) Hematoxylin and eosin (H & E) stained image of corresponding hippocampus tissue. Subcortical white matter with (D) TPM, (E) CARS and (F) H & E stained tissue image. Cellular components and neural fibers are visible in TPM, while myelinated neural fiber was dominantly imaged in CARS images.

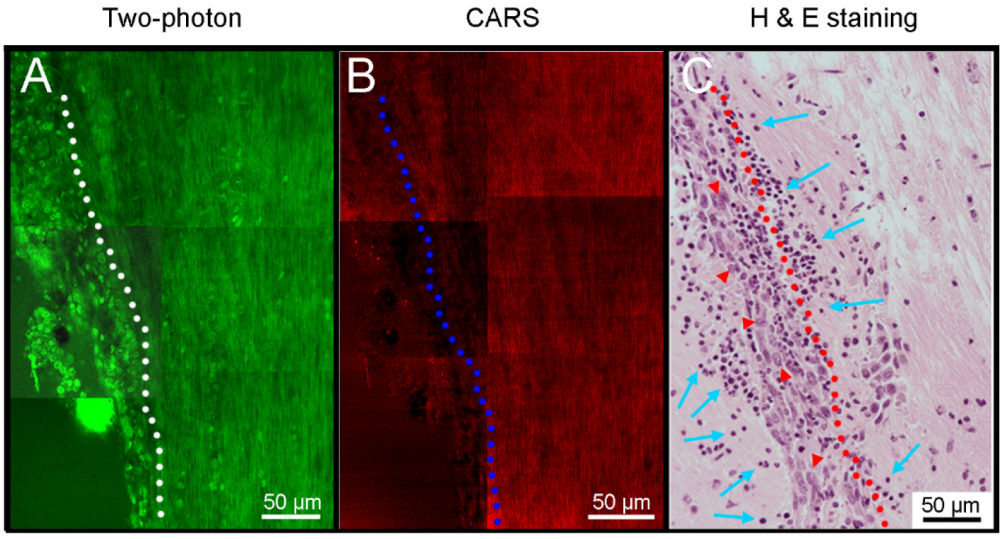

Fig. 4. Mosaic images with TP/CARS microscopy at the vicinity of a metastatic brain tumor. (A) TP image showed significantly higher cellular density region in the left side of white-dotted line. (B) CARS image showed decreased signal in the left side of blue-dotted line. (C) Hematoxylin and eosin (H & E) stained tissue image showed tumor cells (red arrow head) in the left side of red-dotted line. Immune cells were infiltrated to tumor and peritumoral areas (blue arrows).

Next we attempted to image mouse brain sections containing metastatic tumor with commercial TPM to get a large field image with moxifloxacin. Brain tumor was detected in the left cerebral hemisphere of the mouse brain tissue and grossly appeared to penetrate into

Biomedical Optics EXPRESS

the contralateral hemisphere (Fig. 5(a)). TPM image was obtained 20 min after applying moxifloxacin to sliced brain tissue. High cellular density lesion with normal adjacent brain tissue was observed in the green channel (Fig. 5(b) or see Visualization 1). Red fluorescence labeled SL4-DsRed cancer cells were detected in highly concentrated tissue area in the red channel (Fig. 5(c)). Merged image of both the green and red channels confirmed the boundary of metastatic tumor (Fig. 5(d)). For more detailed analysis, four regions of interest (ROIs) were selected and displayed with magnified views (Fig. 5(e)). A part of hippocampus was specifically discernible due to the presence of a distinct curved shape, consisting of pyramidal neurons (Fig. 5(f)). A circular cell cluster, presumably a perivascular metastatic growth, showed higher cellular density than adjacent normal brain tissue (Fig. 5(g)). Inside of tumor (Fig. 5(h)) and tumor border adjacent to normal tissue (Fig. 5(i)) showed higher cellular density with unorganized fashion than adjacent normal brain tissues.

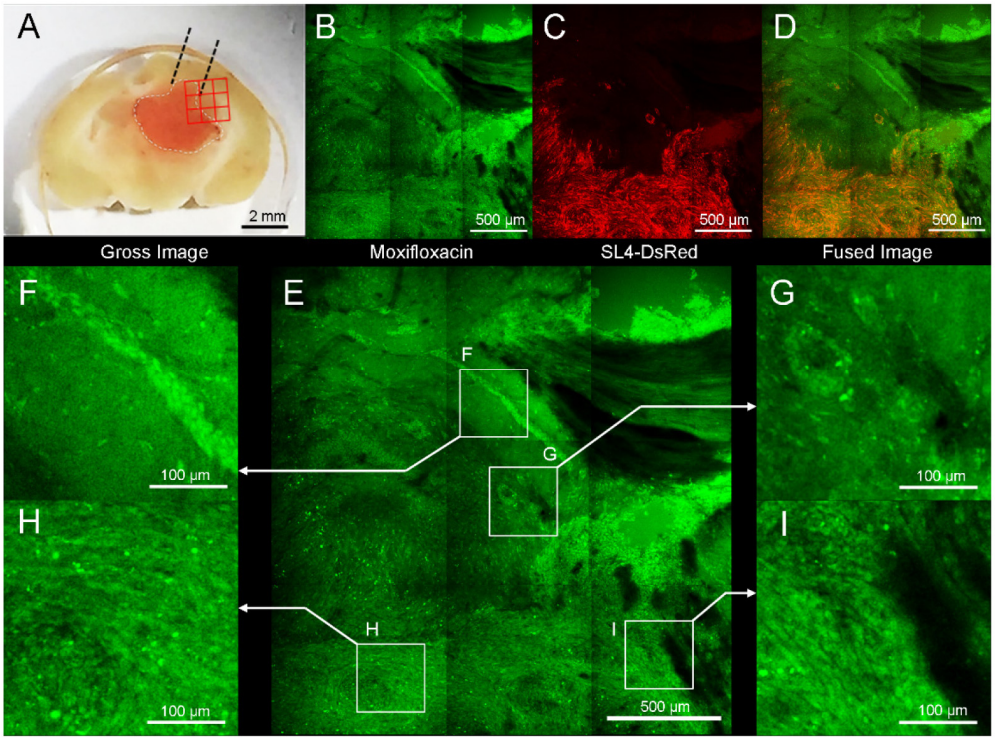

Fig. 5. Moxifloxacin-based TPM image of mouse brain that contains metastatic tumor. (A) SL4-DsRed tumor was mainly located ln left cerebral hemisphere. Red 3 × 3 rectangular region was imaged with TPM. (B) TPM image after topically treated moxifloxacin (green). (C) TPM Red fluorescence image confirming by Ds-Red labeled cancer cells. (D) Merged fluorescence image with moxifloxacin and SL4-DsRed. (E) Four regions of interest (ROIs) are magnified: (F) Multiple cellular bodies were detected in hippocampus. (G) Round, condensed cellular structure was shown. (H) Tumor lesion showed high cellular density. (I) Border of tumor and normal tissue. The cellular density of tumor area was significantly higher than adjacent normal tissue.

To confirm these findings from TPM, we performed hematoxylin and eosin (Figs. 5(h) and 5(e)) staining with the adjacent tissue section. A histological image showed a condensed cellular mass invading into normal adjacent brain tissue (Fig. 6(a)). A magnified image showed perivascular tumor infiltration (Fig. 6(b)). Inside of tumor showed high cellular density (Fig. 6(c)), compared with contralateral normal hippocampus brain tissue (Fig. 6(d)).

Biomedical Optics EXPRESS

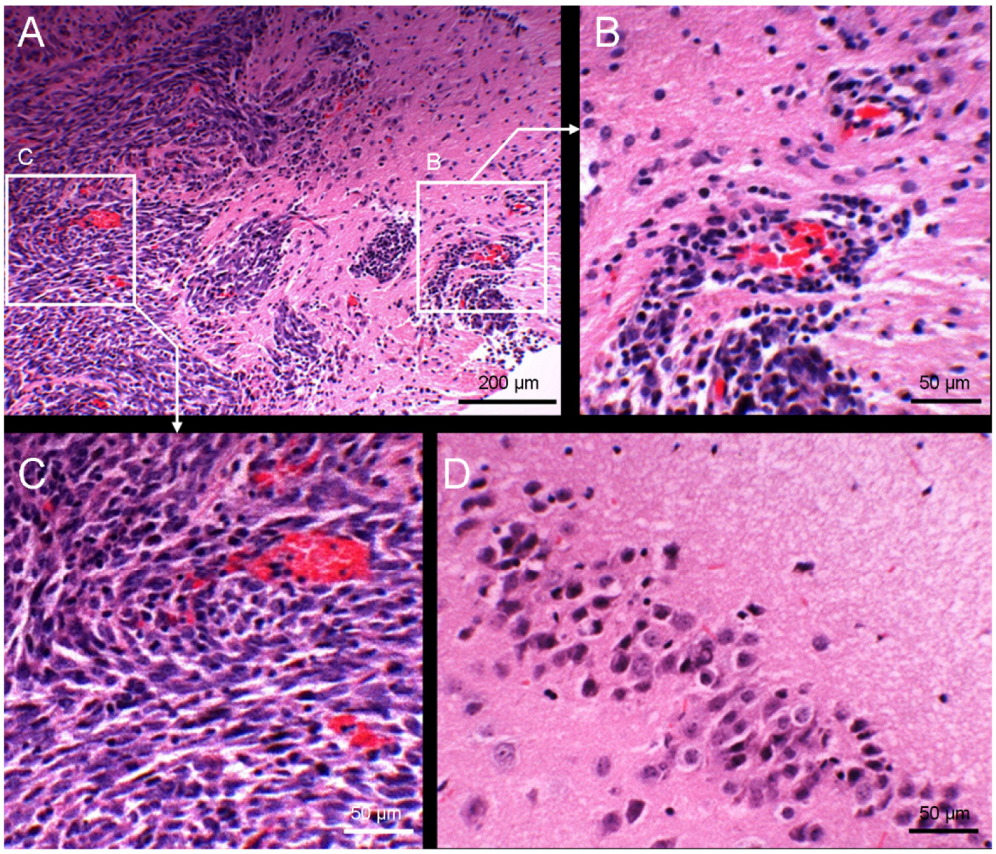

Fig. 6. Histologic characteristics of metastatic brain tumor.(A) H & E staining showed high cellular density tumor cells invading adjacent normal brain tissue (100X). (B) Magnified image showed perivascular growth of metastatic tumor cells along blood vessels evidenced by red blood cells (230X). (C) Magnified image of center of tumor lesion (230X). (D) Hippocampus image in the contralateral normal brain tissue (230X).

With another slice of the same sample, TP images was compared with CARS images to evaluate tumor margin delineation as described in Fig. 7. TP image showed significantly different cellular densities between tumor and adjacent normal tissue. The tumor tissue with densely packed cell bodies can be clearly demarcated with adjacent normal brain tissue that only contains sparsely distributed cell bodies (Fig. 7(a)). CARS image showed higher lipid signals in adjacent normal tissue while diminishing lipid signals at tumor site mainly due to the destruction of myelin (Fig. 7(b)).

4. Discussion and conclusion

In this study, we developed a combined TP/CARS microscopy system, and demonstrated moxifloxacin-based TPM could be used for brain tumor margin delineation with the supplementary from CARS microscopy. To our knowledge, this is the first report to use moxifloxacin as the contrast agent of TPM to delineate brain tumor.

Biomedical Optics EXPRESS

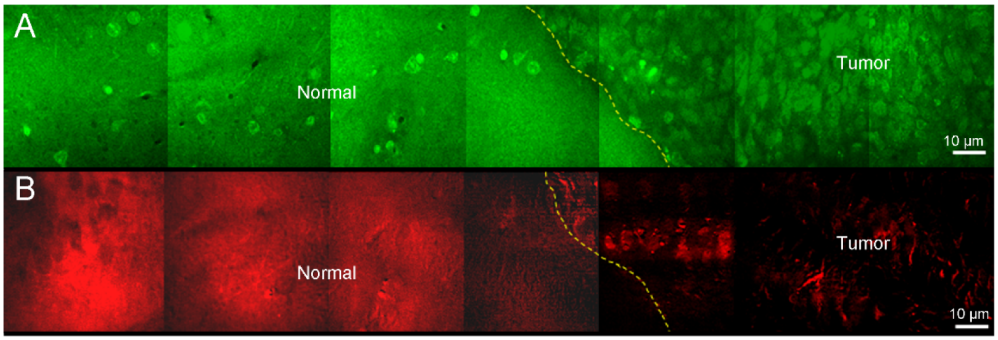

Fig. 7. A strip of images with TP/CARS microscopy at the vicinity of a metastatic brain tumor. (A) TP image showed significantly higher cellular density in tumor region than adjacent normal brain tissue. Numerous cellular body was identified in tumor tissue, while few cellular bodies were shown in adjacent normal tissue. Tumor margins was clearly defined as yellow dotted line. (B) CARS image showed high signal in adjacent normal brain tissue than tumor tissue. Tumor margins was clearly defined as yellow dotted line.

To demonstrate this application to brain tumor, we developed a novel calvarial door approach for intracerebral injection of tumor cells. By opening the door made on the skull and washing the surface after tumor cell injection, we minimized the potential extracerebral tumor growth from leaked cells. This approach provides a reliable and reproducible model system for further study such as cancer treatment efficacy.

Delineation of brain tumor margin was attempted with several optical imaging modalities, such as optical coherence tomography (OCT) [12], diffuse reflectance imaging [6,13] and SRS [25]. While OCT and diffuse reflectance imaging allow relatively large field of view and imaging depth in millimeters, these cannot provide high resolution for cellular level imaging that can result in potential inaccuracy in tumor delineation at infiltrating site. SRS microscopy can provide cellular resolution and biochemical information. However, SRS requires more complex instrumentation than CARS. With combined TP/CARS system, the moxifloxacin-labeled TPM provides high-resolution histoarchitectures and CARS further adds biochemical differentiation such as lipid signal from myelination or lipid droplets improving diagnostic accuracy in the clinic.

The developed TP/CARS combined microscopy system provided subcellular resolution images of both moxifloxacin-labeled cells and myelinated axons. In the current system, the narrow excitation band-pass filter was not added to 808 nm pump beam to maximize the moxifloxacin TP excitation process of the femtosecond laser. However, this approach might increase the CARS background due to the broad spectral bandwidth of femtosecond laser. The narrow band-pass filter could be used if two types of image were acquired sequentially. Furthermore, because moxifloxacin is a FDA-approved compound, the clinical applications of the moxifloxacin-based TP/CARS microscopy could be developed as an intraoperative imaging tool. The combined system would be used to examine both the excised brain tissue and remaining exposed tissue in the surgical field to determine whether there are remnant cancer cells.

The complementary nature of TPM and CARS microscopy may provide enhanced information for tumor margin detection. Both microscopic imaging modalities clearly detected tumor margin from adjacent normal brain tissue (yellow dotted line in Figs. 7(a) and 7(b)). TPM with moxifloxacin clearly showed cellular structure with bright fluorescence, and could detect tumors by visualizing infiltrating high cellular density lesion. On the other hand, label-free CARS microscopy clearly visualized myelinated axons which contained a high density of ordered CH_2 groups which produce a large CARS signal [29]. Due to the destruction of normal brain tissue by the comparatively highly cellular, lipid deficient metastatic tumor cells, the tumor can be discerned by low CARS signal intensity in the CARS

Biomedical Optics EXPRESS

image [23]. With co-registered images of TPM and CARS microscopy, tumor margins may be better identified with combined imaging system.

We also obtained contralateral hemisphere of metastatic brain tumor model with commercial TPM to identify the presence of cancer cell involvements. Moxifloxacin-based TPM images showed high cellular density lesion from adjacent normal brain tissue (Fig. 8(b) in the Appendix or see Visualization 2). Magnified image showed irregularly arranged cells on the brain tissue (Figs. 8(h) and 8(i)). Red fluorescence image from SL4-DsRed cells confirmed that these regions are sites of tumor cell invasion. Due to highly metastatic tendency of SL4-DsRed cells, micro metastasis or cellular infiltration could be revealed with moxifloxacin-based TPM imaging.

In our previous reports, we used 780 nm or 790 nm as an excitation light for moxifloxacin [26, 30]. The peak excitation and emission wavelengths of moxifloxacin is 290 nm and 500 nm, respectively [26]. However, we used 830 nm laser as excitation light to achieve better tissue penetration and simultaneously excite both moxifloxacin and SL4-DsRed fluorescence. In TP/CARS system, we used 808 nm pump beam as excitation light for moxifloxacin to get both CARS and moxifloxacin based TP images simultaneously. Although these wavelengths – 830 nm and 808 nm – were not ideal peak of both moxifloxacin and DsRed fluorophores, we could obtain adequate fluorescence image due to relatively broad excitation spectrum and strong two-photon fluorescence of moxifloxacin.

There are several kinds of fluorescent agents for fluorescence-guided resection of brain tumors, such as aminolevulinic acid (ALA) induced protoporphyrin IX (PpIX), fluorescein, or nanoparticles [11]. While ALA fluorescence has been clinically used for brain tumor resection, it is relatively costly and must be administered several hours prior to surgery as its mechanism of action is based on tumor metabolism [31]. Fluorescein sodium is a non-specific dye for intraoperative visualization of brain tumor based on a disturbed blood-brain barrier (BBB) that poses a risk of false-positive indication such as surgical trauma [32]. Nanoparticles still has low biocompatibility problem. In comparison, moxifloxacin is a low-cost FDA-approved antibacterial agent that provides a direct morphological information with high contrast via topical administration on the exposed tissue of interest with a potential for brain tumor delineation.

Moxifloxacin is a fourth generation fluoroquinolone antibacterial agent and fluoroquinolones have been commonly reported to cause dizziness, drowsiness, headache and more rarely seizures [33]. The global incidence of CNS symptom with fluoroquinolone was 1-2% [34] However, among the fluoroquinolone agents, moxifloxacin showed little CNS-related adverse effect than other fluoroquinolone agents and even more safe than other categories of antibacterial agents [34, 35]. There have been only two case reports that caused seizure by moxifloxacin since FDA approval on 1999 [36, 37]. Both patients had pre-existing CNS disease and seizures were occurred with systemic administration of moxifloxacin for 3 or 5 days. Unlike these systemic administration, we used moxifloxacin as single, topical administration followed by washout in 20 minutes. Therefore, we can obtain the high contrast image while minimizing the drug-related adverse effect. Nevertheless, moxifloxacin should be used with caution for in vivo intraoperative imaging in the clinic.

While moxifloxacin possesses a great potential for clinical TPM imaging, it is nonspecific cell-labeling agent and cannot provide definitive information about the cell types and cellular functionality. Thus the combination of moxifloxacin-based TPM imaging with other complementary modalities such as simultaneous CARS microscopy or TP fluorescence lifetime imaging prior to moxifloxacin-based TPM would be useful. In the current study with brain tissue, the tumor infiltration or margin was examined based on the disruption of known normal histological features of the brain such as distinct hippocampal cytoarchitecture, cellular arrangements and densities, and white matter axonal bundles. Thus whether our proposed approach can be widely applicable for broader setting needs further studies. Nevertheless, our study suggested that moxifloxacin-based TP/CARS microscopy holds a

Biomedical Optics EXPRESS

great potential for differentiating tumor tissue from adjacent normal brain, and warrants further optimization for the treatment of cancer growing in the brain in surgical setting.

In the long run we believe that this TP/CARS system can be used for intraoperative setting. Currently there remain several technical challenges and further development. Present TP/CARS system has high cellular resolution at the cost of smaller FOVs which needs to be improved. TP/CARS microscopy have imaging depth of several hundred microns which could limit the detection of deep infiltrating tumor cells. Leaked blood during surgical procedure would be an obstacle due to attenuation of signal. Furthermore, the TP/CARS system needs to be miniaturized for either portable hand-held device or adaption to surgical microscope head. Hence, initially it is more feasible for TP/CARS system to be used as a complementary benchtop system to assist pathologists with further information on the excised sample.

Appendix

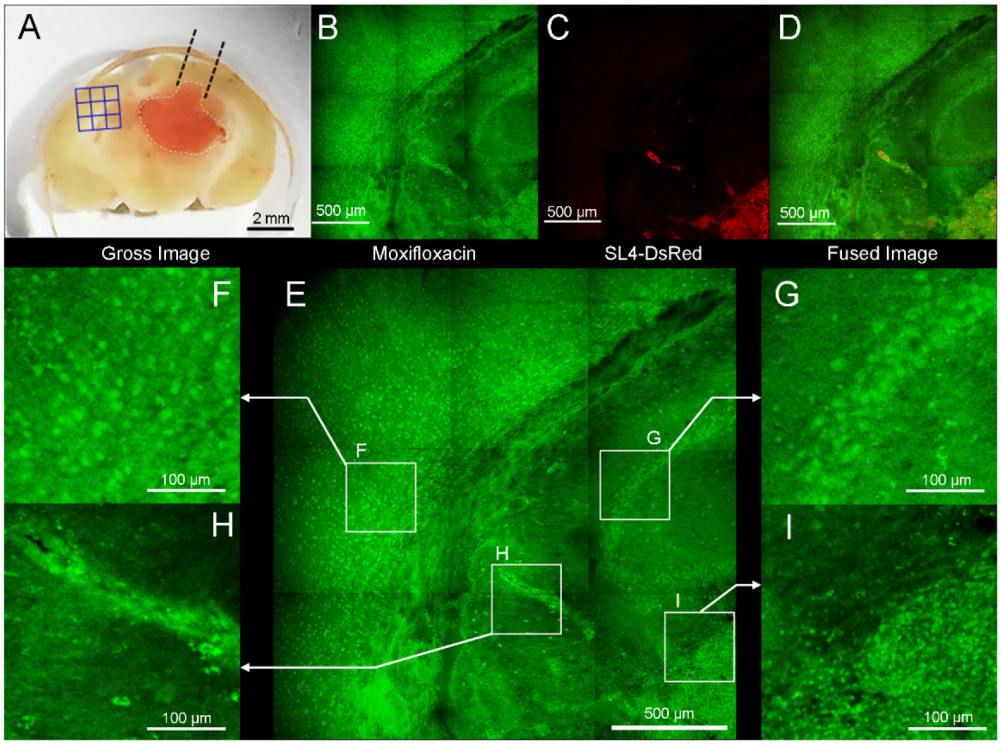

Fig. 8. Moxifloxacin-based TPM image in the contralateral hemisphere of the metastatic brain tumor model. (A) Blue 3 × 3 rectangular lesion were imaged with TPM. (B) TPM image after topically treated moxifloxacin (green). (C) Ds-Red labeled cancer cells were detected with TPM. (D) Merged fluorescence image with moxifloxacin and SL4-DsRed showed metastases of tumor cell to contralateral cerebral hemisphere. (E) Four regions of interest (ROI) are magnified. (F) Multiple cellular bodies were visible. (G) Characteristic cellular array of hippocampus was noticeable. (H) Perivascular tumor growth was identified and confirmed in red fluorescence channel. (I) Border of tumor and normal tissue. High cellular density was identified in tumor area than normal adjacent brain tissue.

Biomedical Optics EXPRESS

Funding

This work was supported in part by the GIST Research Institute (GRI), Biomedical Integrated Technology Research Project, and the GIST-Caltech Research Collaboration Project through a grant provided by GIST in 2017. Also supported by the POSTECH Basic Science Research Institute Grant, Engineering Research Center (No. 2011-0030075), Korea-Sweden Research Cooperation Programme (No. NRF-2014R1A2A1A12067510), research grants (NRF-2011-0019633, NRF-2016R1A2B4015381) of the National Research Foundation (NRF) funded by the Korean government.